We are IntechOpen, the world's leading publisher of Open Access books Built by scientists, for scientists

6,900
Open access books available

185,000
International authors and editors

200M
Downloads

Our authors are among the

154
Countries delivered to

TOP 1%
most cited scientists

12.2%
Contributors from top 500 universities



WEB OF SCIENCE™

Selection of our books indexed in the Book Citation Index in Web of Science™ Core Collection (BKCI)

Interested in publishing with us?
Contact book.department@intechopen.com

Numbers displayed above are based on latest data collected.
For more information visit www.intechopen.com



9

Dispersion Compensation Devices

Lingling Chen, Meng Zhang and Zhigang Zhang
Institute of Quantum Electronics, State Key Laboratory of Advanced Optical Communication Systems and Networks, School of Electronics Engineering and Computer Science, Peking University
P.R.China

1. Introduction

Dispersion compensation plays a key role in generation, amplification and propagation of femetosecond pulses. In the dispersive medium, the pulse can be broaden or compressed depending on the sign of chirp and dispersion. To obtain the ultrashort pulses, the pulse group delay (GD) should have about frequency independence after the dispersion compensation. Especially to compress a pulse to near the transform limit one should not only compensate the GD but also eliminate the high order dispersion term. In this chapter, we briefly review the calculation formulae and design rules of the various dispersive devices including grating and prism pairs and chirped mirrors. An integrative optimization of chirped mirror and its function in mode locked Ti:sapphire laser is described in details. Finally, a useful tool ─ dispersion map is introduced.

2. Grating pairs with negative and positive dispersion

A parallel grating pair as Treacy demonstrated (Fig. 1) can offer a negative group delay dispersion (GDD) (Treacy, 1969). The commonly used phase shift formula through the parallel grating pair is

$$\varphi = \frac{\omega}{c} b(1+\cos\theta) - \frac{2\pi G}{d}\tan(\gamma-\theta)$$

where b and G are the slant and the perpendicular distance path length between the two gratings respectively, d the grating constant, c the speed of light in vacuum, and γ and θ the incident and refraction angle respectively.

For a grating pair with the positive dispersion, Zhang et al (Zhang et al. 1997) proposed a grating- mirror model in contrast to the grating-lens model of Martinez (Martinez, 1987), to demonstrate that the phase shift of a grating-mirror system is a conjugation of that of parallel grating pair. In the model, a mirror with the radius of curvature of R is placed so that the incident point on the grating is right at the circular center of the mirror, as shown in Fig. 2. The simple ray-tracing would result a phase shift as

$$\varphi = \frac{\omega}{c}[4R - b(1+\cos\theta)] + \frac{2\pi G}{d}\tan(\gamma-\theta)$$

Source: Frontiers in Guided Wave Optics and Optoelectronics, Book edited by: Bishnu Pal,
ISBN 978-953-7619-82-4, pp. 674, February 2010, INTECH, Croatia, downloaded from SCIYO.COM

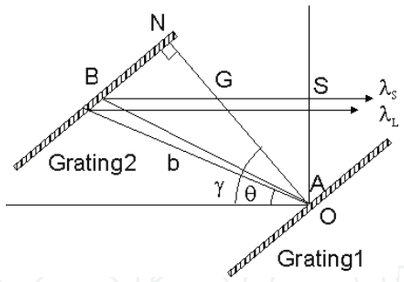


Fig. 1. Treacy grating pair with negative dispersion (adapted from Treacy, 1969)

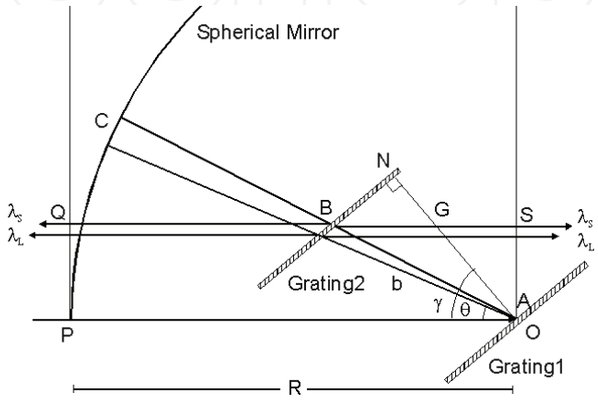


Fig. 2. Graing-mirror with positive dispersion

The subsequent differentiation with respect to frequency results in GD, GDD and the third order dispersion (TOD). Obviously, the only difference between the phase shifts of those two configurations is a constant (4R, depends on the starting point of calculation) and a opposite sign before the term of $b(1+\cos\theta)$. The differentiation would vanish the constant term and leaves an opposite sign. This proves that the grating-mirror configuration is a phase conjugation of the parallel grating pair and can be used as a pulse "stretcher".

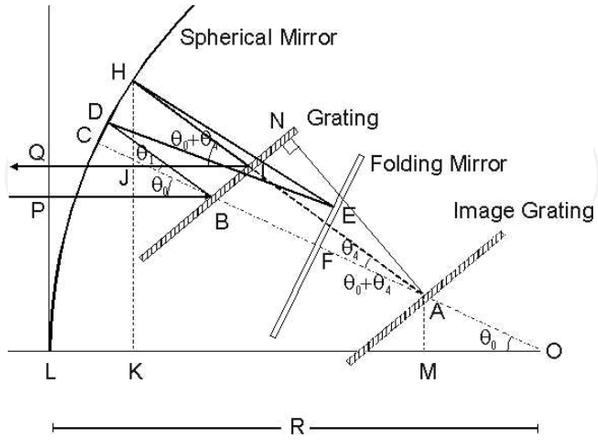


Fig. 3. Folded graing-telescope with positive dispersion

However, this grating-mirror stretcher cannot be realized because, in practice, the incident beam must have a finite size, while the single-mirror system gives no beam collimation. Therefore a telescope is required for the beam collimation.

To derive the similar formula to Equation for the telescope stretcher, we would prefer to start with the folded-grating-telescope stretcher and to adapt it in the coordinate shown in Fig.3. For explicitness, only the incident and the output rays are displayed, the folding mirror and some optical paths have been omitted.

$$\varphi(\omega)=\frac{\omega}{c}(C+A)-\frac{\omega}{c}b\times\left[1+\cos(\theta_0+\theta_4)\right]+\frac{2\pi G}{d}\tan(\gamma-\theta_0-\theta_4)+\frac{2\pi}{d}(G_0-G)\tan(\gamma-\theta_0),$$

where $C=2R-(R-s_1)\cos\theta_0$ is a constant, S_1 =BC, A is an angle dependent variable

$$A=R\left\{\sin(\theta_1-\phi_1)\left(\frac{1}{\sin\theta_1}+\frac{1}{\sin\theta_2}\right)+\sin(\theta_3-\phi_3)\left(\frac{1}{\sin\theta_3}+\frac{1}{\sin\theta_4}\right)\right\}-R\frac{\sin\phi_4}{\sin\theta_4}\cos\theta_0$$

All variables are defined in reference (Zhang et al. 1997).It is noticed that, although the formula is complicated, it takes the form of:

$$\frac{\omega}{c}b\times\left[1+\cos(\theta_0+\theta_4)\right],$$

indicating that it is indeed the phase conjugation of the pulse compressor, except for the mirror induced stigmatism. Similarly, we can have the formulism for Öffner type stretcher, which is (Jiang et al. 2002)

$$\varphi(\omega)=\frac{\omega}{c}(C+A)-\frac{\omega}{c}b\times\left[1+\cos(\theta_0+\theta_6)\right]+\frac{2\pi G}{d}\tan(\gamma-\theta_0-\theta_6)+\frac{2\pi}{d}(G_0-G)\tan(\gamma-\theta_0),$$

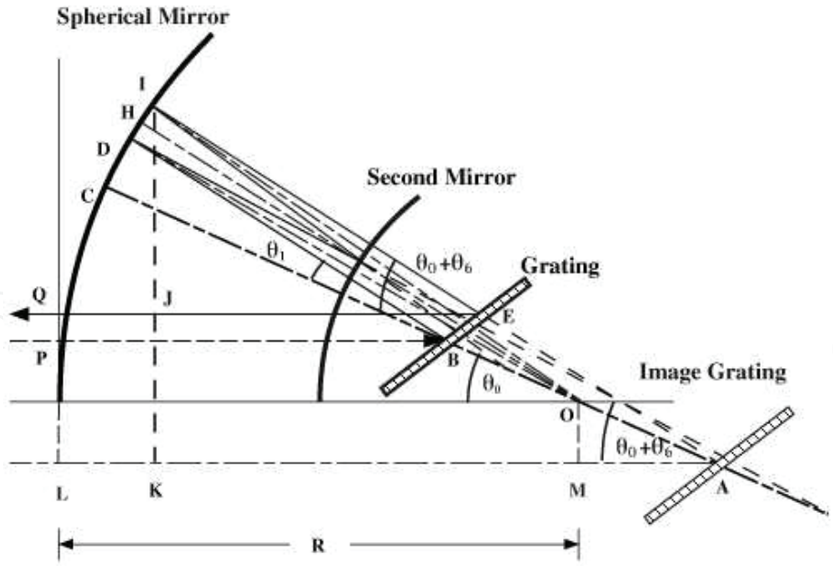


Fig. 4. Öffner type stretcher (adapted from Jiang et al. 2002)

The only difference with Martinez stretcher is the subscript of the angles. All variables are defined in reference (Jiang et al. 2002).

The above formulas, although they are two dimensional, are very useful in optimization of chirped pulse amplification systems.

3. Prism pairs

Prism pairs have also been widely used for dispersion control inside laser oscillators since they can be very low loss in contrast to grating pairs. In 1984 Fork et al. derived formulism of GDD for pair of Brewster-angled prisms (Fork et al. 1984). Nakanuma and Mori noticed that the commonly used formulas developed by Fork were not convenient to use in the case where the adjustable prism insertion is required. They proposed to separate the prism separation and prism insertion (Nakanuma & Mori, 1991) so that those parameters can be easily measured. The simplified formulism is found in reference (Zhang & Yagi, 1993). The GDD and TOD can be expressed to functions of prism separation and prism insertion:

$$\varphi''(\omega) = D_{2L}L + D_{2x}x\,,\quad \varphi'''(\omega) = D_{3L}L + D_{3x}x$$

where the coefficients are approximately

$$D_{2L} = -\frac{2\lambda}{\pi c^2}\lambda\left(\frac{dn}{d\lambda}\right)^2,$$

$$D_{2x} = \frac{2\lambda}{\pi c^2}\lambda^2\frac{d^2n}{d\lambda^2}\frac{1}{n},$$

$$D_{3L} = \frac{3\lambda}{\pi^2 c^3}\left(\lambda\frac{dn}{d\lambda}\right)\left(\lambda\frac{dn}{d\lambda} + \lambda^2\frac{d^2n}{d\lambda^2}\right),$$

$$D_{3x} = -\frac{3\lambda^2}{2\pi^2 c^3}\left(\lambda^2\frac{d^2n}{d\lambda^2} + \frac{\lambda^3}{3}\frac{d^3n}{d\lambda^3}\right)\frac{1}{n}.$$

where n is the refractive index of the prism material. An important advantage of using the above formulism is that they can be presented in a so called dispersion map, as described in section 5.

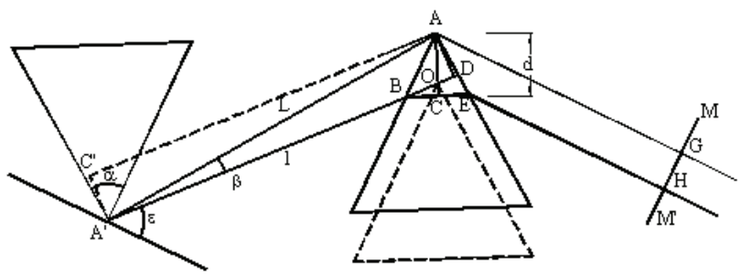


Fig. 5. A typical prism pair arrangement.

4. Chirped mirrors

Although grating and prism pairs are widely used as the compressor schemes, they suffer from high order dispersion. By contrast, chirped mirrors (CMs) which are dispersive multilayer structures designed by optimizing the initial design are usually used for pulses compression by providing dispersion without much material in the beam path. They can provide the precisely controlled GD, GDD, even higher order dispersion such as third order

dispersion (TOD), as well as the high reflectivity in a broadband or ultra-broadband wavelength range. They are key components for extremely short pulse compression and especially have played a critical role in the development of octave-spanning lasers and the generation of mono-cycle pulses. In 2007, 1.5-octave chirped mirrors have been proposed and demonstrated, for extra-cavity compression to 3 fs pulses (Pervak et al. 2007). Furthermore, they are important for compression of attosecond soft-x-ray pulses (Wonisch et al. 2006).

There are always ripples in GDD curves of broadband chirped mirrors, due to the interference between the reflections from different layers of a multilayer structure. Although the ripples can be minimized by the optimization procedure such as with commercially available software, it is difficult to reduce the ripples to acceptable level when the design of a single chirped mirror has to operate over the wavelength ranges up to an octave spanning or more. Therefore, several other approaches to reduce GDD ripples have been proposed, such as double-chirped mirrors (Kärtner et al. 1997; Matuschek et al. 1998; Kärtner et al. 2001), complementary CM pairs (Pervak et al. 2005; Pervak et al. 2007). By pairing the CMs, the dispersion ripples of CMs are opposite to each other. Thus, the residual ripple of the CM pairs could be very small.

The design rule of CMs consists of two main issues. The first issue is the initial multilayer design. The design procedure of chirped mirrors is usually to start with a favorable initial structure, then to perform optimization. In this procedure, the initial design is very crucial. If the initial design is not close enough to the target, the optimization procedure is impossible to reach a satisfactory result. The commonly used initial designs are double chirp (DC) and modulated layer thickness (MLT) (Tempea et al. 1998).

The second issue is the optimization process including the choices of targets and optimization methods. Although a CM is characterized by a certain value of GDD that is the second derivative of the phase shift on reflection with respect to the angular frequency, GD was mostly chosen as the target, because the second derivative of the phase has two problems: the accuracy and the time consumption in the optimization. However, we found that just taking GD as the target cannot ensure a smooth GDD. Besides the targets setting, we should also consider the optimization methods. Although paring two CMs is a good idea to eliminate the ripples but in some cases such as generating octave-spanning in four-mirror Ti:Sapphire ring cavity it is not enough. Then we introduce the intracavity optimization.

4.1 Initial design of chirped mirrors

Here, we summarize two different designs as the initial layer structure for the optimization and compare the differences. First was the DC, and the second was the MLT.

The conception of DC mirrors has been proposed by Käertner (Kärtner et al. 1997; Matuschek et al. 1998) where in addition to the chirp of the Bragg wave number, the thickness of the high refractive index layers is also chirped.

Assuming the double chirped mirrors composed of 2N index steps with high refractive index medium such as TiO_2 and low refractive index medium such as SiO_2. The thicknesses of low index layer are linearly chirped while the thicknesses of high index layer are given by

$$d_{H,i}(x) = \frac{\lambda_{\max}}{4n_H}\left(\frac{N+1-i}{N}\right)^{\eta} \quad \text{where } \eta = 1, 2 \quad i=1,2,\ldots,N+1$$

Where η=1, 2 for linear and quadratic chirp. The clear reduction of oscillations in the GD by the double chirped technique is visible (Matuschek et al. 1998). Moreover, the index-matching can be extended by a properly high quality AR-coating.
MLT method (Tempea et al. 1998) is based on the recognition that in the two component structure, the effects of modulating the layer thickness is similar to that of a corresponding modulation of refractive index. Composing the mirror with narrow bandwidth filters with gradually shifted central wavelength may avoid some resonant interference. The general formula described the variation of the layer thickness is given by

$$t(x) = t_0(x) + A(x)\sin(2\pi \frac{x}{\Lambda(x)})$$

where x is the distance of the respective layer from the substrate and the number of layers within a modulation period Λ must be kept constant,

$$\Lambda(x) = \alpha t_0(x)$$

where the parameter α determines the number of layers within a modulation period and can be set as $\alpha = 5$ (i.e.), equal to its minimum permitted value.
For an early constant negative GDD in the high reflectance range we need

$$t_0(x) = \frac{1}{4}(\frac{\lambda_{\min} - \lambda_{\max}}{d}x + \lambda_{\max})$$

where d is the total optical thickness of the coating. One problem in CM design is to obtain negative GDD at the shortest wavelength of the high-reflectance range. This difficulty is related to that the shortest wavelength components have a limited penetration depth which tends to result in a constant GD. This problem can be alleviated by increasing the amplitude of the modulation depth by

$$A(x) = \frac{A_2 - A_1}{d}x + A_1$$

where A_1, A_2 ($>A_1$) are limits between which the amplitude is allowed to vary.
The above equations consist of a complete recipe of the design of chirped mirror by using MLT method.
We simulated two chirped mirror pairs to compare these two above initial designs—DC (pair 1) and MLT (pair 2) (Chen et al. 2007). The target was CM pairs providing negative GDD of around -50 fs^2 and TOD of around -35 fs^3 at 800 nm with the reasonable residual GDD ripples and high reflectivity in wavelength range of 600-1200 nm. In the DC model, we chose the first order. In the MLT model, the number of layer within a modulation period was 5, the minimum modulation amplitude was 12.5 nm and maximum modulation amplitude was 62.5 nm, same as in the reference (Tempea et al. 1998). The total layer number of each mirror in a pair for both models was 80.
After optimization, from Fig. 6 and 7, we can see that both of the CM pairs meet the target at 800 nm with the residual GDD ripples <15 fs^2 and the reasonable high reflectivity. Meanwhile, we find that the time consuming on optimization for pair 1 is little longer than pair 2, the GDD curve is closer to what we required and the GD is matched better in the spectral range. Particularly, the reflectivity is relatively higher.

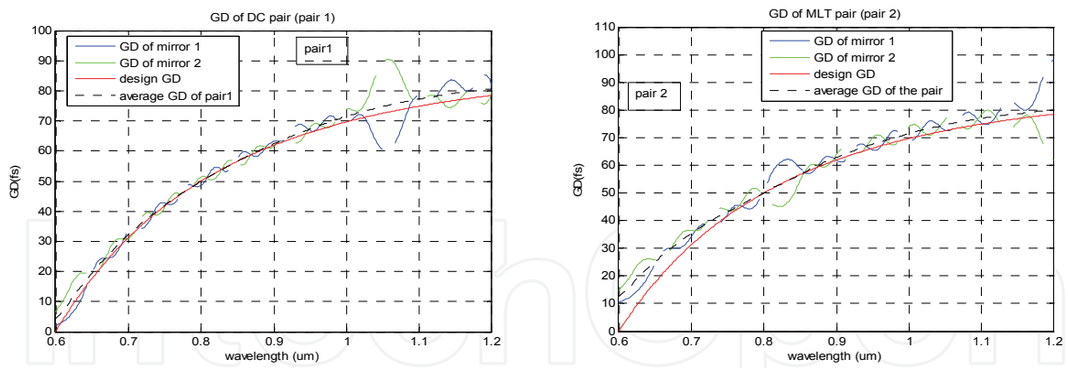


Fig. 6. GD for different design DC mirrors (pair1) and MLT CMs (pair2)

It is noticed that, from Fig. 8 we can see that the reflectivity of pair 1 is above 99.4% in most of spectral range except the 1170~1200 nm. However, reflectivity of pair 2 is unexpectedly low (< 99%) in the range of 810~910 nm. If these CM pairs are going to be used inside laser cavity, the loss of mirrors is one of the most important factors we should consider. In this regard, pair 1 is better than pair 2.

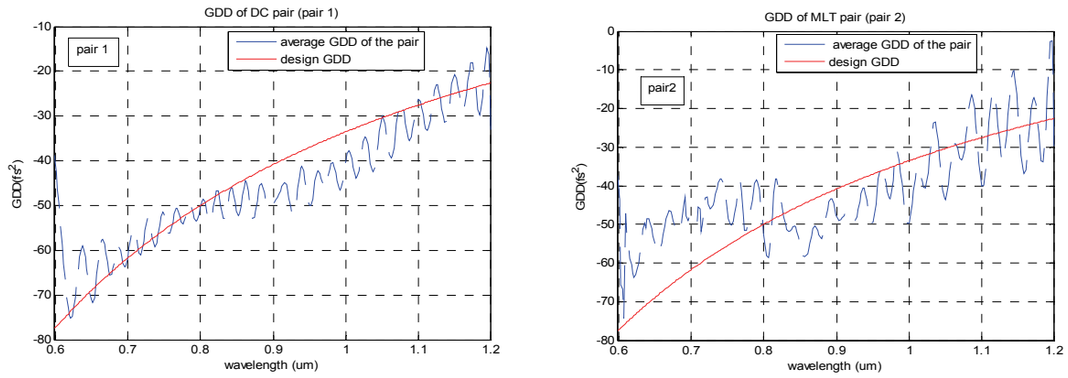


Fig. 7. GDD for different design DC mirrors (pair1) and MLT CMs (pair2)

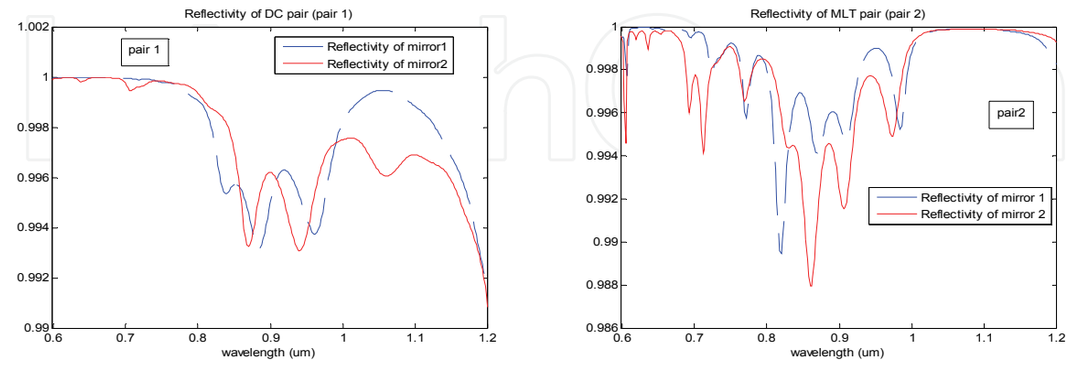


Fig. 8. Reflectivity for different design DC mirrors (pair1) and MLT CMs (pair2)

The above simulation is just one example to design the CM pairs. We can see each initial design has its own advantages and disadvantages; thus, the choice mainly depends on the specific necessities.

4.2 Optimization of chirped mirrors

4.2.1 Optimization targets

It is noticed that in some cases, the two CMs can be better paired with each other with GD as the target than with GDD as the targets (Pervak et al. 2007). For complementary pair mirrors, the merit function is modified as below when we take GD as the target:

$$F = \sum_{i=1}^{n} \left\{ \left[\frac{R_1(i) - R_t(i)}{\Delta R} \right]^{\alpha} + \left[\frac{R_2(i) - R_t(i)}{\Delta R} \right]^{\beta} + \left\{ \frac{\left[GD_1(i) + GD_2(i) \right] / 2 - GD_t(i)}{\Delta GD} \right\}^{\chi} \right\} \tag{1}$$

where the subscripts j = 1, 2 represents each individual mirror. R_t (i) and GD_t(i) are the desired values at the wavelength λ_i . R_j(i) and GD_j(i) are the calculated instantaneous values. ΔR and ΔGD are the corresponding tolerances and n is the number of wavelength points. The weighting parameters α, β and χ, have to be adjusted according to the error in the process to handle the optimization.

We should also notice that CMs are finally characterized by the GDD. Therefore, in the final optimization step, GDD can be used to be the target. The merit function thus takes the following form in this case:

$$F = \sum_{i=1}^{n} \left\{ \left[\frac{R_1(i) - R_t(i)}{\Delta R} \right]^{\alpha} + \left[\frac{R_2(i) - R_t(i)}{\Delta R} \right]^{\beta} + \left\{ \frac{\left[GDD_1(i) + GDD_2(i) \right] / 2 - GDD_t(i)}{\Delta GDD} \right\}^{\chi} \right\} \tag{2}$$

where the variables are the same as in Eq. (1), except GDD in the place of GD.

Considering these two aspects, we find that the optimization process can be divided into three steps. In the first and second optimization, the GD and GDD are set to be the optimization target respectively, as described in Eq. (1) and Eq. (2), where the derivative of the phase is calculated by the Birge and Kaertner method (Birge et al. 2006), since this method reduces the calculation time. During the third optimization, the exact differential process is applied for fine adjustment for the target of GDD.

4.2.2 Optimization methods

As we said before, to minimize the ripples in GDD curves of broadband chirped mirrors, especially ones operate over the wavelength ranges up to an octave spanning or more, people developed complementary CM pairs. However, in the octave-spanning lasers, particularly in the high repetition rate (~1 GHz) ring cavity lasers (Fortier et al. 2006; Nogueira et al. 2006), there are three CMs and one output coupler. Two of the CMs are usually paired, but the other one has no mirror to pair with. Therefore, the total dispersion is usually heavily oscillated, and the compensation is incomplete in such a laser (Fortier et al. 2006; Nogueira et al. 2006). The same difficulty also happens to the linear cavity, where the end mirrors offer one bounce reflection while other CMs experience twice which can be designed in pair. Silver mirror has been used as the end mirror to avoid this problem (Matos et al. 2004). However, the high reflection loss and the weak durability of the silver mirror make the laser inefficient and short-lived. Though octave spanning spectrum has been obtained by some groups with such a cavity, it requires quite a critical alignment. Therefore, more precise overall intracavity dispersion compensation scheme has to be developed.

In 2008, a new cavity for octave-spanning laser is proposed by the MIT group (Crespo et al. 2008), where two pairs of chirped mirrors (four chirped mirrors) were designed and

combined to obtain quite a low ripple of the intracavity GDD. The output coupler, however, was performed by the coating on a fused-silica wedge. Sub-two-cycle pulses were obtained.
In 2009, another method for precise intracavity dispersion compensation: the integrative optimization of all cavity mirrors, provided that the output coupler has a flat GDD (Chen et al. 2009) is proposed by us. Both GDD and TOD were considered. This technique allows minimizing the ripples of the whole GDD for ultra-broadband femtosecond lasers.
Take an example as in four-mirror Ti:Sapphire ring cavity for this intracavity optimization to obtain the octave spanning. The four-mirror ring cavity for optimization is shown in Fig. 9. In an octave-spanning Ti:Sapphire laser, one or two mirrors have to have a low reflectivity at 532 nm for the pumping beam to go through while to maintain a high reflectivity from 600 nm to 1200 nm. This constrict makes the oscillation of the GDD larger than the other mirrors. Therefore, we first designed this pump mirror, and then matched the dispersion of this mirror with the other two mirrors. After that, we optimized these three mirrors together with all requirements (reflection and GDD). In Fig. 9, M1 and M2 are concave mirrors. M1 is the pump mirror. M3 may be a convex mirror (Fortier et al. 2006; Nogueira et al. 2006). The optimization procedure for two mirrors was similar to that in reference (Crespo et al. 2008), but with more steps as described below.

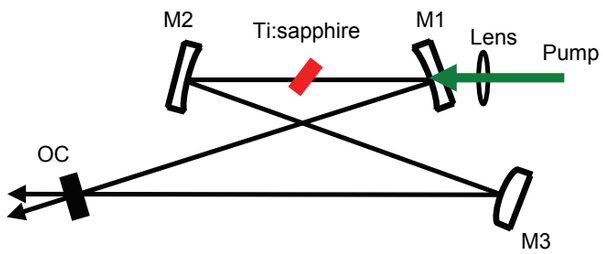


Fig. 9. Schematic of four-mirror ring cavity. M1, M2 and M3 are chirped mirrors for integrative dispersion optimization; OC is the output coupler.

The reflectivity of the pump mirror M1 was designed to be less than 20% in the wavelength range of 500-540 nm, particularly less than 5% at 532 nm. The reflectivity of the other two mirrors was set without the restriction on the transmission at 532 nm. The reflectivity of all the mirrors was maintained to be more than 99.8% in the desired spectral range of 600-1200 nm. The target GDD and TOD of each CM were set to be -50 fs^2 and -35 fs^3 at the central wavelength of 800 nm so as to compensate the dispersion employed by the 2.3 mm Ti:Sapphire crystal (The GDD employed by the output coupler is assumed to be zero). For all other wavelengths the GD and GDD were calculated respectively, as for the optimization target of 351 points in the wavelength range of 500-1200 nm. The initial design of all mirrors was adapted from the double chirped mirror. The optimization process was adapted as we said in 4.2.1, which was divided into 3 stages and merit functions were modified as below:

$$F=\sum_{i=1}^{n}\left\{\left[\frac{R_1(i)-R_t(i)}{\Delta R}\right]^{\alpha}+\left[\frac{R_2(i)-R_t(i)}{\Delta R}\right]^{\beta}+\left[\frac{R_3(i)-R_t(i)}{\Delta R}\right]^{\gamma}+\left\{\frac{\left[GD_1(i)+GD_2(i)+GD_3(i)\right]/3-GD_t(i)}{\Delta GD}\right\}^{\chi}\right\}$$

$$F=\sum_{i=1}^{n}\left\{\left[\frac{R_1(i)-R_t(i)}{\Delta R}\right]^{\alpha}+\left[\frac{R_2(i)-R_t(i)}{\Delta R}\right]^{\beta}+\left[\frac{R_3(i)-R_t(i)}{\Delta R}\right]^{\gamma}+\left\{\frac{\left[GDD_1(i)+GDD_2(i)+GDD_3(i)\right]/3-GDD_t(i)}{\Delta GDD}\right\}^{\chi}\right\}$$

The final optimization results for all CMs are shown in Fig. 10 and Fig. 11. Figure 10 shows that the reflectivity of M1 has a high transmission at 532 nm, and all three mirrors have the reflectivity more than 99% for the wavelength range of 600-1200 nm. It also shows that the combined GD of the three mirrors agrees well with the desired GD curve. This in turn results in a best fit with the GDD curve (Fig. 11). The GDD ripples of the combined three mirrors are less than 25 fs² for most wavelengths from 600 to 1200 nm. This is in comparison with the unbalanced mirror dispersion in reference (Fortier et al. 2006), where ripples of net GDD were as high as more than 100 fs².

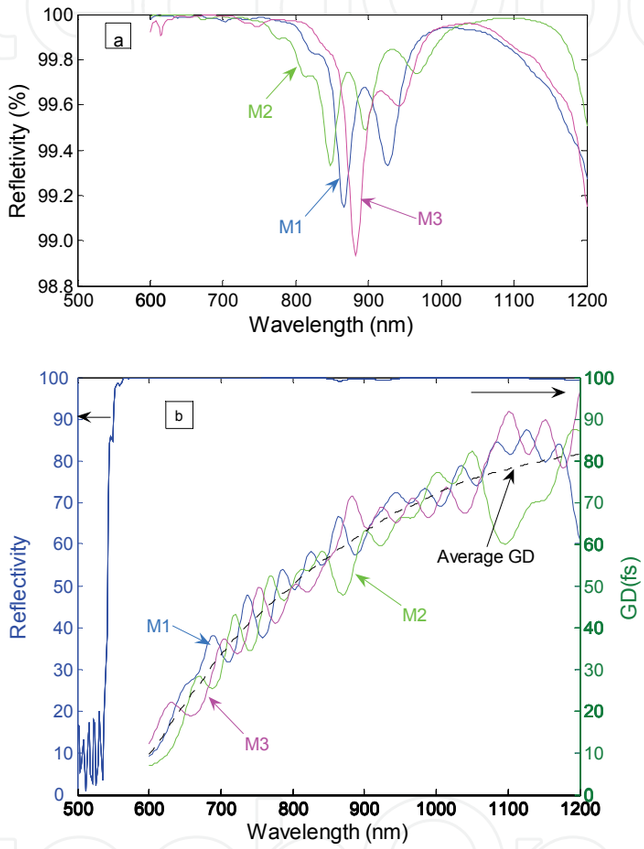


Fig. 10. (a) Reflectivity of each CM. (b) Individual and combined average GD (GD1+GD2+GD3)/3) of three CMs.

Although the combined GDD is smooth and flat, the large ripple of GDD in each individual mirror is still a concern that may destroy the pulse evolution. To testify the pulse profile changes on those mirrors, we introduce a pulse on the three mirrors in sequence and look at the pulse evolution. The pulse is assumed to be secant hyperbolic and chirp-free with spectrum of 696–904 nm, corresponding to a transform-limited pulse of 8 fs (FWHM). For each CM, a constant GDD is added so that the GDD at 800 nm is based to be 0 fs². In this way, the effect of the GDD ripples on the pulse could be clearly seen. When this pulse goes to those three mirrors in the order of M1, M2, and M3, the pulse duration becomes 8.21 fs, 8.80 fs, 9.31 fs and the corresponding energy in the main pulse is 97.14%, 92.89%, and 92.24% of the initial value respectively (Fig.12). When three mirrors are combined together, the

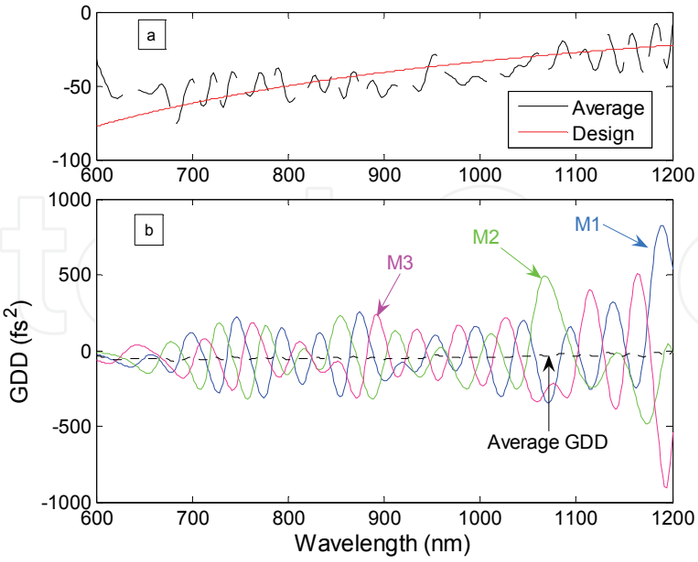


Fig. 11. (a) Combined and averaged GDD ((GDD1+GDD2+GDD3)/3) of three CMs. The solid curve is the designed GDD. (b) Individual and averaged GDD of three mirrors in a larger scale.

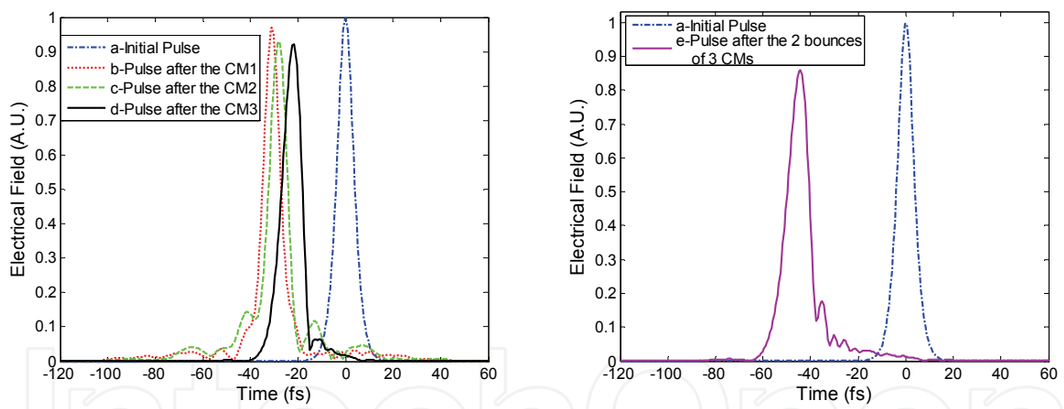


Fig. 12. Temporal analysis of the reflection of an incident secant hyperbolic-shaped free-chirp 8-fs pulse (a) from the CMs. The curve (b), (c), (d) correspond to the envelope of the pulse reflected from M1, M2, M3 orderly after one bounce, (e) reflected from the three CMs after two bounces. The temporal shift of the curves is artificial. Notice that a constant GDD is added to each CM to base the GDD at 800 nm to be 0 fs^2, so that the effect of the GDD ripples on the pulse could be clearly seen.

pulse width becomes 9.31 fs after one bounce and 10.53 fs after two bounces. The energy in the main pulse is 85.86% of the initial value after two bounces. It is noticed that slight satellite pulses appear after two bounces but the pulse still maintains its shape (Fig. 12), indicating that the residual GDD ripples of these three CMs do not destroy the pulse.

In a laser cavity, the pulse is circulating and the accumulated GDD ripples may destroy the pulse formation. However, the amplitude modulation caused by Kerr lens mode locking

plays also an important role in pulse shaping. We simulated the pulse evolution in the Ti: Sapphire laser cavity with the master equation (Haus et al. 1992). The Kerr lens mode locking was modeled as a saturable absorber described by

$$q(a) = q_0 / (1 + |a|^2 / P_A) \quad \text{(Kärtner et al. 2005)},$$

where a is the electrical field, q_0 the modulation depth, and P_A the saturation fluence of the absorber. By solving the master equation, we obtained a stable solution for the pulse profile. The intracavity pulse spectrum expands from 600 nm to 1200 nm at about 20 dB, shown in Fig. 13. The simulation demonstrated that the ultrashort pulses in the Ti:Sapphire laser would ultimately build up in such a cavity without pulse splitting or collapse and the intracavity GDD would be compensated well with these three CMs.

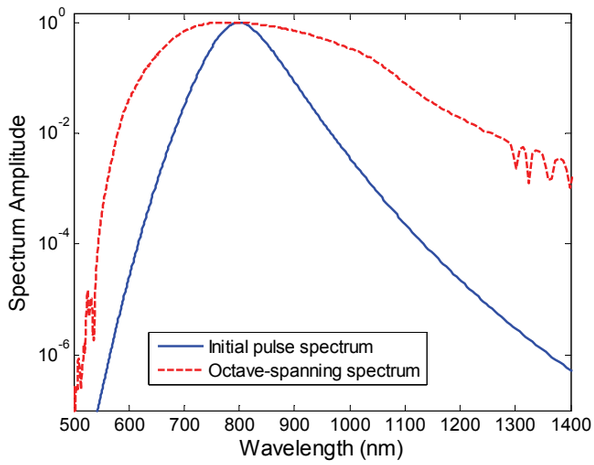


Fig. 13. The shaping of a pulse iteratively propagated in the ring cavity of Ti:Sapphire laser in frequency domain.

The inconvenience of this scheme in practice is that one additional mirror has to be coated separately, in addition to the chirped mirror pair. This will increase the manufacturing cost as well as the risk of phase errors resulted from imperfect coating. Nevertheless, the new scheme should be able to significantly reduce uncontrolled ripples and hopefully to achieve octave-spanning spectrum easier than using unbalanced mirrors.

In summary, we noticed from the simulation that this multi-mirror simultaneous optimization technique can reduce the total cavity dispersion ripples in a ring cavity. This technique allows minimizing the ripples of the whole GDD for ultra-broadband femtosecond lasers. This technique is able to easily extend to the design of chirped mirrors in linear cavities, where the number of bounces is difficult to match for paired mirrors. Another logical extension of this technique is the design of multi-chirped-mirror set for over one octave-spanning spectrum for extra-cavity dispersion compensation.

5. Mapping dispersion for compensation

In order to show how the dispersion is compensated in a laser system, or in any other extracavity dispersion compensation scheme, Nakanuma et al introduced a so-called

dispersion "map" where the second order and the third order dispersion are expressed in a orthogonal coordinates (Nakanuma et al. 1991). The second order dispersion is the horizontal while the third order dispersion is in the vertical coordinate respectively. This map is very useful in selecting dispersion compensation schemes.

Let us take an example. In a Ti:Sapphire laser, if we only consider the dispersion introduced by the sapphire crystal, its second and third order dispersion are fs^2 and fs^3 respectively. In the map, the dispersion can be expressed in a vector with the horizontal and vertical coordinates of (Nakanuma et al. 1991). The purpose of using this map is to basically bring the vector back to zero, by introducing prism pairs. The prism pair dispersion depends on the prism separation and insertion, which are not independent. However, by the geometry introduced in section 3, for the crystal length of 20 mm, the dispersions could be

$$D_2 = -26.7l + 471.6d$$

$$D_3 = -63.2l + 320.9d$$

that is, in the map, the prism pair dispersion can be expressed by two vectors: one represent the prism separation dependent and the other is the prism insertion dependent. One can chose the prism separation and the prism insertion to make the total dispersion zero. As indicated in reference (Zhang et al. 1997), this can be made by solving equations

$$D_{2l}l + D_{2d}d + D_{2g} = 0$$

$$D_{3l}l + D_{3d}d + D_{3g} = 0$$

To obtain finite and positive solutions of l and d, D_{2t}, D_{3t}, D_{2d} and D_{3d} should satisfy either condition 1:

$$R_l > R_g \quad \text{and} \quad R_d > R_l$$

or condition 2:

$$R_l < R_g \quad \text{and} \quad R_d < R_l$$

where $R_l = D_{3l} / D_{2l}$ and $R_d = D_{3d} / D_{2d}$

In Ti:sapphire crystal, at the wavelength of 800 nm, the slope of the crystal is 0.7 fs; if we chose SF10 glass prism pair (A_1-B_1-C_1), the slope R_l and R_d are 1.71 fs and 0.69 fs and respectively. They cannot satisfy either condition, therefore the vector is open. One can choose prism material with R_l and R_d as small as possible, such as fused silica (A_1-B_2-C_2). However, because the unit dispersion is smaller too, the required prism separation would be enormously long that is not acceptable in a laser cavity. The only choice is to shorten the crystal length so that the residual third order dispersion is minimized (A_2-B_3-C_3) for the shortest pulse generation.

However, as the laser operation wavelength changes, the corresponding material dispersion changes, as well as the dispersion slope does. In this case, the map can help choosing the prism materials, if a prism pair is preferred. For example, a Cr:forsterite laser, which the operation wavelength is 1300 nm, the slope of the dispersion is 3.8 fs, much higher than at

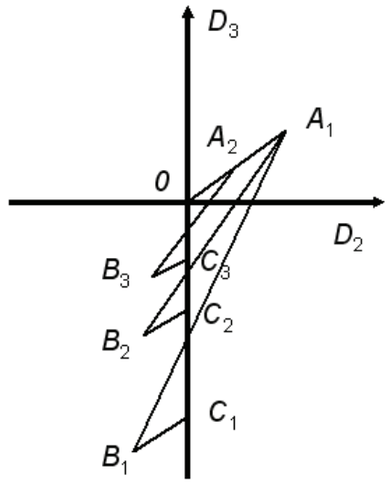


Fig. 14. Dispersion mapping for Ti:Sapphire crystal

800nm. Figure x shows a typical map for forsterite at 1290 nm. The gain material dispersion D_{2g} and D_{3g} are drawn as a vector *OA*, which shows a significantly steep slope in the map. By investigation, most of the prism materials available do not fulfill condition 1: $R_l > R_g$, but fit to $R_l < R_g$. Therefore, we have to search for the materials which satisfy the second part of condition 2: $R_d < R_l$. Some of the materials do satisfy condition 2 such as SFS01, SF58, and SF59. In the map, the dispersion of a SFS01 prism pair is drawn as another vector AB and BC which bring the gain dispersion vector back to origin so that the net D_2 and D_3 are simultaneously zero, to complete a triangle loop. The prism separation *l* and the insertion *d* can be derived from section 3. The dispersion vector of the SF14 prism pair is also plotted in dashed lines in Fig. 15 as a comparison. Apparently it is not possible to complete the triangle using the SF14 prism pair at this wavelength and a net positive TOD will remain in the cavity. The vectors for SF6 prisms (not plotted) will also end up with a net positive TOD because of $R_d \approx R_l$. Checking the wavelength dependence of the dispersion material, we found that SF14 at a wavelength shorter than 1230 nm satisfies the condition 2: $R_d < R_l$. Therefore, it is reasonable to choose SF14 prisms as the dispersion compensator for the laser operated at a shorter wavelength than 1230 nm. If either condition 1 or condition 2 can be satisfied, there should be no severe restriction on the gain crystal length. This is particularly good for Cr:forsterite because its low thermal conductivity does not allow to use a thin crystal with high doping density. It is reasonable to use a relatively long crystal to ease the thermal problem (Ivanov et al 1995). This is in contrast to the case of Ti:sapphire lasers where neither of the conditions can be fulfilled by available prism materials so that thin crystal is the only choice.

In the wavelength of 1550 nm, the dispersion slope of the Cr:YAG crystal increases to >11 fs. There are no more glass materials making the prism pair have such a high slope. One can draw the map as in Fig. 15 and will find that any glass material will leave a positive and high TOD. Rather, simply a piece of fused silica itself would do the compensation of second order only (Ishida & Naganuma, 1994), because its bulk material has a negative second order and positive third order, while the fused silica prism pair does not offer a negative

third order by increasing the prism separation. Therefore, either prism pair or bulk material will ultimately make the third order positive.
It should be noted that, in an inhomogeneously broadened laser medium, such as Nd:glass, this map does not work well, because it requires much more dispersion to make it mode locked (Lu et al. 2001).

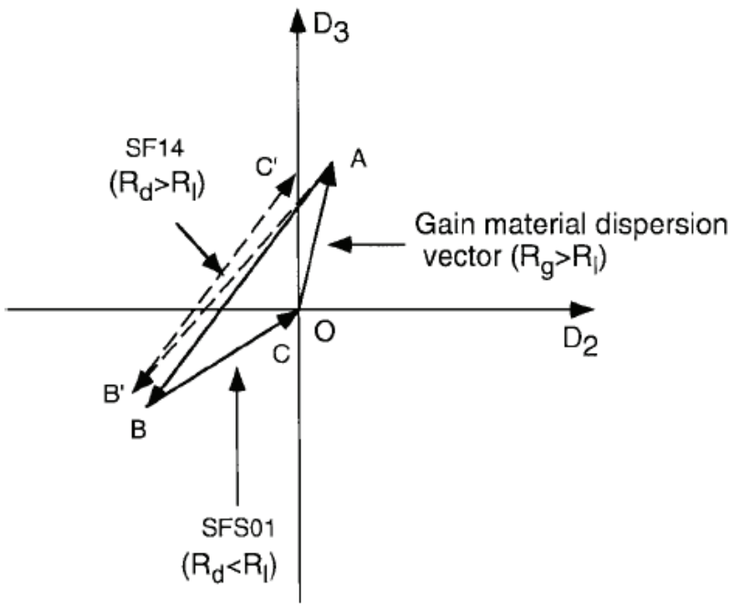


Fig. 15. Intracavity dispersion mapping for Cr:forsterite crystals

The similar method can be applied into the chirped pulse amplifier (CPA). In a grating stretcher (O-A_1) compressor (A_2-A_3) system with identical incident angle and slant distance,

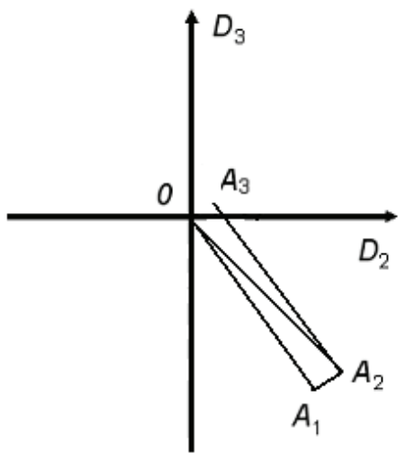


Fig. 16. Dispersion mapping for a CPA system

the material dispersion (A_1-A_2) plays a key role in breaking the balance (i.e., bring the dispersion to the origin) of dispersion introduced by grating pairs. The necessity of compensating the third order dispersion (A_2-O) can be very obvious in the map.

6. Conclusions

We have reviewed three important dispersion compensation devices including grating pair, prism pair and chirped mirrors. We also summarized the detailed calculation formulism for readers' convenience. The emphasis was given to the novel design of chirped mirrors. Finally, a dispersion map was introduced for conveniently mapping intracavity and extracavity dispersions of a femtosecond laser or an amplification system.

7. References

Birge, J. R.; & Kaertner, F. X. (2006). "Efficient analytic computation of dispersion from multilayer structures". *Appl. Opt.* 45(7): 1478~1483, ISSN: 0003-6935

Chen, L.; & Zhang, Z. "Design of broadband chirped mirrors with different initial designs". *Conference on Lasers and Electro-Optics/Pacific Rim 2007,* paper TuB1_5, ISBN: 978-1-4244-1173-3, Korea, Aug. 2007, Seoul.

Chen, L.; Yang, W.; Wang, X. & Zhang, Z. (2009). "Integrative optimization of chirped mirrors for intracavity dispersion compensation". *Opt. Commun*. 282(4): 617~620, ISSN: 0030-4018

Crespo, H. M.; Birge, J. R.; Falcão-Filho, E. L.; Sander, M. Y.; Benedick, A. & Kärtner, F. X. (2008). "Nonintrusive phase stabilization of sub-two-cycle pulses from a prismless octave-spanning Ti:sapphire laser". *Opt. Lett*. 33(8): 833~835, ISSN: 0146-9592

Fork, R. L.; Martinez, O. E. & Gordon, J. P. (1984). "Negative dispersion using pairs of prisms". *Opt. Lett*. 9(2):150~152, ISSN: 0146-9592

Fortier, T. M.; Bartels, A. & Diddams, S. A. (2006). "Octave-spanning Ti:sapphire laser with a repetition rate >1 GHz for optical frequency measurements and comparisons". *Opt. Lett*. 31(7): 1011~1013, ISSN: 0146-9592

Haus, H. A.; Fujimoto, J. G. & Ippen, E. P. (1992). "Analytic theory of additive pulse and Kerr lens mode locking ". *IEEE J. Quantum Electron.* 28(10): 2086~2096, ISSN: 0018-9197

Ishida, Y. & Naganuma, K. (1994). "Characteristics of femtosecond pulses near 1.5 μm in a self-mode-locked Cr4+:YAG laser". *Opt. Lett*. 19(23): 2003~2005, ISSN: 0146-9592

Ivanov, A. A.; Minkov, B. I.; Jonusauskas, G.; Oberle, J. & Rulliere, C. (1995). "Influence of Cr4+ in concentration on cw operation of forsterite laser and its relation to thermal problems". *Opt. Commun*. 116(1-3): 131~135, ISSN: 0030-4018

Jiang, J.; Zhang, Z. & Hasama, T. (2002). "Evaluation of chirped-pulse-amplification systems with Offner triplet telescope stretchers". *J. Opt. Soc. Am. B*, 19(4): 678~683, ISSN: 0740-3224

Kärtner, F. X.; Matuschek, N.; Schibli, T.; Keller, U.; Haus, H. A.; Heine, C.; Morf, R.; Scheuer, V.; Tilsch, M. & Tschudi, T. (1997). "Design and fabrication of double-chirped mirrors". *Opt. Lett.* 22(11): 831~833, ISSN: 0146-9592

Käertner, F. X.; Morgner, U.; Schibli, T. R.; Ippen, E. P.; Fujimoto, J. G.; Scheuer, V.; Angelow, G. & Tschudi, T. (2001). "Ultrabroadband double-chirped mirror pairs for generation of octave spectra". *J. Opt. Soc. Am. B* 18(6): 882~885, ISSN: 0740-3224

Kärtner, F. X.; Ippen E. P. & Cundiff, S. T. (2005). "Femtosecond Laser Development,", In: "*Femtosecond Optical Frequency Comb: Principle, Operation, and Applications*," Ye, J. and Cundiff, S. T. (Ed.), 54~75, Springer, ISBN: 0-387-23790-9, Boston.

Lu, W.; Yan, L. & Menyuk, C. R. (2001). "Kerr lens mode locking of Nd:glass laser," *Opt. Commun*. 200(1-6): 159~163, ISSN: 0030-4018

Martinez, O. E. (1987). "3000 times grating compressor with positive group velocity dispersion: Application to fiber compensation in 1.3-1.6 μm region". *IEEE J. Quantum Electron.* QE-23(1): 59~64, ISSN: 0018-9197

Matos, L.; Kleppner, D.; Kuzucu, O.; Schibli, T. R.; Kim, J.; Ippen, E. P. & Kaertner, F. X. (2004). "Direct frequency comb generation from an octave-spanning, prismless Ti:sapphire laser''. *Opt. Lett*. 29(14): 1683~1685, ISSN: 0146-9592

Matuschek, N.; Kärtner, F. X. & Keller, U. (1998). "Theory of double-chirped mirrors". *IEEE J. Select. Topics Quantum Electron.*4(2): 197~-208, ISSN: 1077-260X

Naganuma, K. & Mogi, K. (1991). "50-fs pulse generation directly from a colliding-pulse mode-locked Ti:sapphire laser using an antiresonant ring mirror". *Opt. Lett*. 16(10): 738~740, ISSN: 0146-9592

Nogueira, G. T. & Cruz, F. C. (2006). "Efficient 1 GHz Ti:sapphire laser with improved broadband continuum in the infrared". *Opt. Lett*. 31(13): 2069~2071, ISSN: 0146-9592

Pervak, V.; Naumov, S.; Tempea, G.; Yakovlev, V.; Krausz, F. & Apolonski, A. (2005). "Synthesis and manufacturing the mirrors for ultrafast optics". *Proc. SPIE* 5963 (59631P). ISSN: 0277-786X

Pervak, V.; Tikhonravov, V.; Trubetskov, M. K.; Naumov, S.; Krausz, F. & Apolonski, A. (2007). "1.5-octave chirped mirror for pulse compression down to sub-3 fs". *Appl. Phys. B* 87(1): 5 ~12, ISSN: 0946-2171

Tempea, G.; Krausz, F.; Spielmann, Ch. & Ferencz, K. (1998). "Dispersion control over 150 THz with chirped dielectric mirrors". *IEEE J. Selec. Topics in Quan. Electron.*, QE-4(2): 193~196, ISSN: 0018-9197

Treacy, E.B. (1969). "Optical Pulse Compression with Diffraction Gratings". *IEEE J. Quantum Electron.* QE-5(9), 454~458, ISSN: 0018-9197

Wonisch, A.; Neuhäusler, U.; Kabachnik, N. M.; Uphues, T.; Uiberacker, M.; Yakovlev, V.; Krausz, F.; Drescher, M.; Kleineberg, U. & Heinzmann, U. (2006). "Design, fabrication, and analysis of chirped multilayer mirrors for reflection of extreme-ultraviolet attosecond pulses". *Appl. Opt.* 45(17): 4147~4156, ISSN: 0003-6935

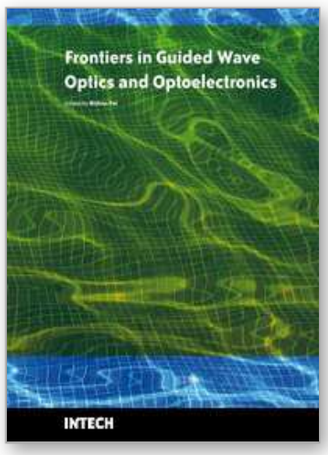
Zhang, Z.; Yagi, T. & Arisawa, T. (1997). "Ray-tracing model for stretcher dispersion calculation". *Appl. Opt.* 36(15): 3393~3399, ISSN: 0003-6935

Zhang, Z. & Yagi, T. (1993). "Observation of group delay dispersion as a function of the pulse width in a mode locked Ti:sapphire laser". *Appl. Phys. Lett*. 1993, 63(22): 2993~1995, ISSN: 0003-6951

Zhang, Z.; Torizuka, K.; Itatani, T.; Kobayashi, K.; Sugaya, T. & Nakagawa, T. (1997). "Femtosecond Cr:forsterite laser with mode locking initiated by aquantum-well saturable absorber". *IEEE J. Quantum Electron*. QE-33(11): 1975~1981, ISSN: 0018-9197.

IntechOpen

IntechOpen



Frontiers in Guided Wave Optics and Optoelectronics

Edited by Bishnu Pal

ISBN 978-953-7619-82-4
Hard cover, 674 pages
Publisher InTech
Published online 01, February, 2010
Published in print edition February, 2010

As the editor, I feel extremely happy to present to the readers such a rich collection of chapters authored/co-authored by a large number of experts from around the world covering the broad field of guided wave optics and optoelectronics. Most of the chapters are state-of-the-art on respective topics or areas that are emerging. Several authors narrated technological challenges in a lucid manner, which was possible because of individual expertise of the authors in their own subject specialties. I have no doubt that this book will be useful to graduate students, teachers, researchers, and practicing engineers and technologists and that they would love to have it on their book shelves for ready reference at any time.

How to reference

In order to correctly reference this scholarly work, feel free to copy and paste the following:

Lingling Chen, Meng Zhang and Zhigang Zhang (2010). Dispersion Compensation Devices, Frontiers in Guided Wave Optics and Optoelectronics, Bishnu Pal (Ed.), ISBN: 978-953-7619-82-4, InTech, Available from: http://www.intechopen.com/books/frontiers-in-guided-wave-optics-and-optoelectronics/dispersion-compensation-devices

INTECH
open science | open minds

InTech Europe
University Campus STeP Ri
Slavka Krautzeka 83/A
51000 Rijeka, Croatia
Phone: +385 (51) 770 447
Fax: +385 (51) 686 166
www.intechopen.com

InTech China
Unit 405, Office Block, Hotel Equatorial Shanghai
No.65, Yan An Road (West), Shanghai, 200040, China
中国上海市延安西路65号上海国际贵都大饭店办公楼405单元
Phone: +86-21-62489820
Fax: +86-21-62489821

© 2010 The Author(s). Licensee IntechOpen. This chapter is distributed under the terms of the Creative Commons Attribution-NonCommercial-ShareAlike-3.0 License, which permits use, distribution and reproduction for non-commercial purposes, provided the original is properly cited and derivative works building on this content are distributed under the same license.

IntechOpen

IntechOpen